MOLECULAR AND CELLULAR BIOLOGY, Aug. 2004, p. 6719–6727 Vol. 24, No. 15
0270-7306/04/$08.00+0 DOI: 10.1128/MCB.24.15.6719–6727.2004

Gene-Targeted Mice Lacking the Trex1 (DNase III) 3′→5′ DNA Exonuclease Develop Inflammatory Myocarditis

Masashi Morita,[1]† Gordon Stamp,[2] Peter Robins,[1] Anna Dulic,[1] Ian Rosewell,[1] Geza Hrivnak,[1] Graham Daly,[1] Tomas Lindahl,[1]* and Deborah E. Barnes[1]

Cancer Research UK, London Research Institute, Clare Hall Laboratories, South Mimms, Hertfordshire EN6 3LD,[1] and Department of Histopathology, Faculty of Medicine, Imperial College, London W12 0NN,[2] United Kingdom

Received 11 February 2004/Returned for modification 29 February 2004/Accepted 1 May 2004

TREX1, originally designated DNase III, was isolated as a major nuclear DNA-specific 3′→5′ exonuclease that is widely distributed in both proliferating and nonproliferating mammalian tissues. The cognate cDNA shows homology to the editing subunit of the *Escherichia coli* replicative DNA polymerase III holoenzyme and encodes an exonuclease which was able to serve a DNA-editing function in vitro, promoting rejoining of a 3′ mismatched residue in a reconstituted DNA base excision repair system. Here we report the generation of gene-targeted *Trex1*$^{-/-}$ mice. The null mice are viable and do not show the increase in spontaneous mutation frequency or cancer incidence that would be predicted if Trex1 served an obligatory role of editing mismatched 3′ termini generated during DNA repair or DNA replication in vivo. Unexpectedly, *Trex1*$^{-/-}$ mice exhibit a dramatically reduced survival and develop inflammatory myocarditis leading to progressive, often dilated, cardiomyopathy and circulatory failure.

Two distinct nuclear exonucleases account for the major part of the total exonucleolytic activity on DNA observed in mammalian cell extracts (24, 25). They were identified as a 3′→5′ exonuclease acting preferentially on single-stranded DNA and a 5′→3′ exonuclease specific for double-stranded DNA that could remove a single-stranded 5′ overhang as an oligonucleotide. These nuclear enzymes were designated DNase III and DNase IV, as they are distinct from the pancreatic and macrophage lysosomal DNA endonucleases DNase I and DNase II. DNase IV was later renamed flap endonuclease 1 (FEN1) (23), and its main function is processing displaced 5′ single strands that arise during lagging-strand DNA replication, as well as during DNA repair, recombination, and triplet repeat expansion. The elimination of Fen1 activity leads to early embryonic lethality in mice, consistent with an essential role of the enzyme in DNA replication (20). In contrast, DNase III is expressed at similar levels in nonproliferating and proliferating tissues; it was isolated as the major nuclear 3′→5′ DNA exonuclease from the adult rabbit liver (14) and also from the calf thymus and human myoblasts, where it was designated TREX1 (37, 38).

The human TREX1/DNase III cDNA (14, 29) shares amino acid sequence homology with the *Escherichia coli* DnaQ/MutD editing subunit of the replicative DNA polymerase III holoenzyme, which can increase the fidelity of an exonuclease-deficient mammalian DNA polymerase in vitro (36). The TREX1/DNase III cDNA encodes a nonprocessive 3′→5′ DNA-specific exonuclease, with a preference for single-stranded DNA or mispaired 3′ termini; like the native protein isolated from mammalian cells, it forms homodimers (14, 29, 30). Since two of the major mammalian nuclear DNA polymerases, Polα and Polβ, do not have an intrinsic 3′ exonuclease function, it was proposed that TREX1/DNase III may serve to edit mismatched deoxyribonucleotides during lagging-strand DNA synthesis or gap filling in DNA base excision repair, which are conducted by Polα and Polβ, respectively (14, 29, 30). It was previously shown that recombinant TREX1/DNase III can edit a 3′ mismatch in an in vitro base excision repair system reconstituted with Polβ (14). Other 3′ exonuclease activities have also been described that can apparently proofread for Polα or Polβ (3, 43). Furthermore, a modest 3′→5′ exonuclease activity of the APE1/HAP1 apurinic-apyrimidinic (AP) endonuclease, which interacts with Polβ (2), can apparently edit mismatched nucleotides that are erroneously incorporated by Polβ, in addition to its major incision role in base excision repair (5, 51), at least in vitro, but the significance of this exonuclease activity remains unclear (6, 22, 50). Such 3′ exonuclease activities might also moderate the efficacy of antiviral or anticancer compounds based on 3′ blocking nucleoside analogues (7, 37, 38).

In addition to TREX1/DNase III, several other autonomous (i.e., non-DNA polymerase-associated) 3′→5′ exonucleases have been reported for mammalian cells, with apparent roles in DNA repair, DNA recombination, or DNA damage checkpoint control (for a review, see reference 42). This is in contrast to the 5′→3′ exonucleases, of which only FEN1 and the mismatch repair nuclease EXO1 have been described, both of which are targeted in the mouse (20, 48). The mammalian 3′ exonucleases include TREX2, which, like TREX1/DNase III, is expressed in all tissues examined and shares ~44% amino acid identity with TREX1, but it lacks a unique C-terminal extension of 68 amino acids that is present in TREX1 (29, 31). Our knowledge of the biochemical properties of these enzymes, their interactions with other proteins, and their

* Corresponding author. Mailing address: Cancer Research UK, London Research Institute, Clare Hall Laboratories, South Mimms, Hertfordshire EN6 3LD, United Kingdom. Phone: 44-207-269-3993. Fax: 44-207-269-3819. E-mail: lindahl@cancer.org.uk.

† Present address: Banyu Tsukuba Research Institute, Tsukuba, Ibaraki 300-2611, Japan.

physiological function(s) remains limited; several, including TREX2, have been characterized only as recombinant proteins, and for others, such as APE1, their major role may be unrelated to their 3′ exonuclease activity (22). These autonomous enzymes may assist exonuclease-proficient DNA polymerases under adverse conditions; for example, TREX2 interacts with Polδ and may increase its fidelity when deoxynucleoside triphosphate pools are unbalanced (42). The importance of this group of enzymes to genetic stability is illustrated by the premature aging of Werner syndrome patients, who are deficient in the WRN 3′→5′ exonuclease (15), and the cancer susceptibility of proofreading-defective Polδ mutant mice (13).

TREX1/DNase III is a major nuclear 3′→5′ exonuclease in mammalian cells, with no orthologue in lower eukaryotes such as yeasts. We propose that the terminology of Mazur and Perrino (29) be adopted and henceforth refer to the protein as TREX1 (3′ repair exonuclease 1). In order to elucidate the function of this enzyme in vivo, we have generated and characterized gene-targeted *Trex1*$^{-/-}$ mice.

MATERIALS AND METHODS

Generation of *Trex1*$^{-/-}$ mice and cell lines. Gene-targeted *Trex1*$^{-/-}$ knockout mice were generated by standard techniques, essentially as described previously (19). The murine *Trex1* open reading frame (ORF) was isolated by reverse transcription-PCR (RT-PCR) based on available sequences from the expressed sequence tag databases (GenBank). The full-length murine *Trex1* cDNA was subsequently cloned and expressed (29). The cDNA probe was used to screen a murine 129/Ola genomic cosmid library, and two positive clones were identified (MPMGc121O02220Q2 and MPMGc121G24675Q2; Resource Center of the German Human Genome Project [http://www.rzpd.de]). One of these clones (MPMGc121O02220Q2) was used to produce the targeting construct, and restriction enzyme mapping, together with Southern hybridization analysis with the cDNA probe above, showed that there were no introns within the murine *Trex1* ORF. The targeting strategy to disrupt the murine *Trex1* gene is shown schematically in Fig. 1A. An ~0.3-kb PstI fragment encoding amino acids 103 to 207 of the *Trex1* ORF product, including conserved exonuclease Mg^{2+}-binding motifs II and III (14, 29), was replaced by a neomycin resistance gene and polyadenylation signal (*neo* cassette) from pMC1Neo PolyA (Stratagene). The *neo* cassette and flanking genomic fragments were subcloned into the multiple cloning site of the pBluescript II SK vector by standard techniques. The targeting construct was verified by restriction enzyme mapping and DNA sequencing and was propagated in the SURE *E. coli* strain (Stratagene).

The targeting construct was linearized with Asp718 and electroporated into GK129 embryonic stem (ES) cells from 129Sv mice. Genomic DNAs from G418-resistant colonies were screened by Southern hybridization analysis with a flanking probe and by PCR with flanking primers, using the strategies shown in Fig. 1. ES clones in which homologous recombination had occurred in one allele of the *Trex1* gene were injected into blastocysts from C57BL/6J mice, the resultant chimeras were mated, and agouti F_1 progeny that were heterozygous for the *Trex1* allele (+/−) were interbred to produce F_2 progeny (Fig. 1B and C). The mice were maintained under specific-pathogen-free conditions, their ages at death were recorded, and systematic macroscopic postmortem analyses were done for all mice. Primary mouse embryonic fibroblasts (MEFs) were established from day 13.5 embryos, and permanent cell lines were established from spontaneously transformed clones arising after repeated passaging in culture by standard techniques.

Genotyping of mice and RNA analysis. All mice were genotyped from tail-snip biopsy samples. Southern hybridization analysis with a 3′ flanking XbaI-PstI genomic fragment as a probe (Fig. 1A and B) was performed by standard procedures. PCR genotyping (Fig. 1A and C) used primer 1 (sense; 5′-CGGG ATCCGATGACAACCTGGCCATCCTGCTCCGAG-3′), primer 2 (antisense; 5′-CCTGCCATTGCTGGGACTTCCATTG-3′), and Ex*Taq* according to the manufacturer's instructions (TaKaRa Biomedicals) for 30 cycles of 94°C for 30 s, 68°C for 30 s, and 72°C for 2 min. For RT-PCR analysis of the *Trex1* mRNA, total RNAs were isolated from spleens of *Trex1*$^{-/-}$ and *Trex1*$^{+/+}$ mice and reverse transcribed by use of an RNA extraction kit and a first-strand synthesis kit (Amersham Biosciences). PCR amplification of nonsaturating amounts of the *Trex1* transcript was performed by using the primers described above, in parallel with control amplification of a fragment of the same size from the glyceraldehyde-3-phosphate dehydrogenase transcript.

Preparation of cell extracts, antibodies, and enzyme assays. Nuclear extracts of mouse tissues or MEFs were prepared as described previously (19). Briefly, cell suspensions were lysed in 2 volumes of hypotonic buffer A (10 mM HEPES-KOH [pH 7.7], 0.5 mM $MgCl_2$, 10 mM KCl, 1 mM dithiothreitol [DTT], 0.2 mM phenylmethylsulfonyl fluoride). Nuclei were recovered by centrifugation (2,000 × *g* for 10 min) and extracted in 2 volumes of high-salt buffer B (20 mM HEPES-KOH [pH 7.7], 0.5 mM $MgCl_2$, 420 mM NaCl, 0.2 mM EDTA, 1 mM DTT, 0.2 mM phenylmethylsulfonyl fluoride, 25% glycerol). After centrifugation (14,000 × *g* for 10 min), the supernatant was recovered and dialyzed against 25 mM HEPES-KOH (pH 7.7)–1 mM DTT (buffer C) containing 50 mM KCl, divided into aliquots, and snap-frozen in liquid nitrogen. Alternatively, the crude nuclear extract was dialyzed into buffer C containing 100 mM NaCl and 10% glycerol and then was further purified by column chromatography on single-stranded DNA cellulose (Amersham Biosciences) equilibrated in the same buffer. The column was washed in buffer containing 400 mM NaCl and the bound proteins were eluted with 1.5 M NaCl, or serial fractions were collected in an increasing salt gradient (200 mM to 1.4 M) applied in 200 mM steps. Enzyme assays were performed as described previously (14). The poly(dA) substrate was 3′ end labeled by the incorporation of [^{32}P]dAMP by terminal transferase (Amersham Biosciences). Reaction mixtures (50 μl) contained 0.01 μg of the 3′-end-labeled poly(dA) substrate in 50 mM Tris-HCl (pH 8.5), 4 mM $MgCl_2$, 1 mM DTT, and 5 μg of bovine serum albumin. After incubation at 37°C for 30 min, the substrate was ethanol precipitated, with the addition of 50 μg of denatured calf thymus carrier DNA, and the radioactive material released into the supernatant was determined by scintillation counting.

Antibodies were raised against a murine-specific synthetic peptide corresponding to amino acids 220 to 233 of the 304-residue Trex1 protein; only 6 of these 14 amino acids are conserved in the human ORF product, and since this epitope is located where the extended C-terminal region of Trex1 diverges, only 4 residues are common to murine Trex2 (14, 29). An N-terminal cysteine residue was included, the peptide was coupled to hemocyanin, and antibodies were raised and affinity purified by standard procedures. Proteins separated by sodium dodecyl sulfate–12% polyacrylamide gel electrophoresis were transferred to nitrocellulose membranes, incubated with diluted antibody (1:600), and detected by chemiluminescence using a derivatized secondary antibody (ECL Western blotting analysis system; Amersham Biosciences).

Analysis of spontaneous mutagenesis in vivo. *Trex1*$^{-/-}$ null mice were established in a homozygous *Big Blue* background, and the spontaneous mutation frequency in vivo was analyzed as described previously (19), except that the response of the *cII*, rather than *lacI*, nontranscribed transgene was assayed by using the λ Select-*cII* mutation detection system (Stratagene). Appropriate null and wild-type animals were sacrificed at 5 weeks of age, and the integrated lambda shuttle vector was recovered, packaged into viable bacteriophages, and used to infect the appropriate *E. coli* host. Bacteriophages (~500,000) were plated at 24°C for 40 h (selective conditions) to identify *cII*$^{-}$ mutants that were unable to undergo lysogeny. Putative *cII*$^{-}$ mutant plaques were verified by replating them at a low density under selective conditions. The mutation frequency was calculated as the ratio of mutant plaques to the total number of PFU screened, with the latter being estimated from dilutions plated at 37°C for 18 h (nonselective conditions).

Histopathology. Dissected tissues were fixed in 10% formalin and embedded in paraffin, and sections were stained with hematoxylin and eosin. Immunohistochemistry was performed with mouse antibodies specific for the B-cell marker CD45R and the pan-T-cell marker CD3 (Pharmingen), followed by anti-mouse immunoglobulin G (IgG) coupled to a streptavidin-biotin complex, and staining was detected by incubation with diaminobenzidine.

RESULTS

Generation of gene-targeted *Trex1*$^{-/-}$ null mice. Homozygous *Trex1*$^{-/-}$ null mice were generated by targeted disruption of the *Trex1* gene in ES cells. Members of our laboratory previously isolated a human cDNA encoding a catalytically active 304-amino-acid recombinant gene product (14). The sequence encoding amino acids 103 to 207 was replaced with a *neo* cassette in the targeting construct (Fig. 1A). This deleted motifs II and III of three conserved exonuclease sequence motifs containing Mg^{2+}-binding aspartic acid residues that are required

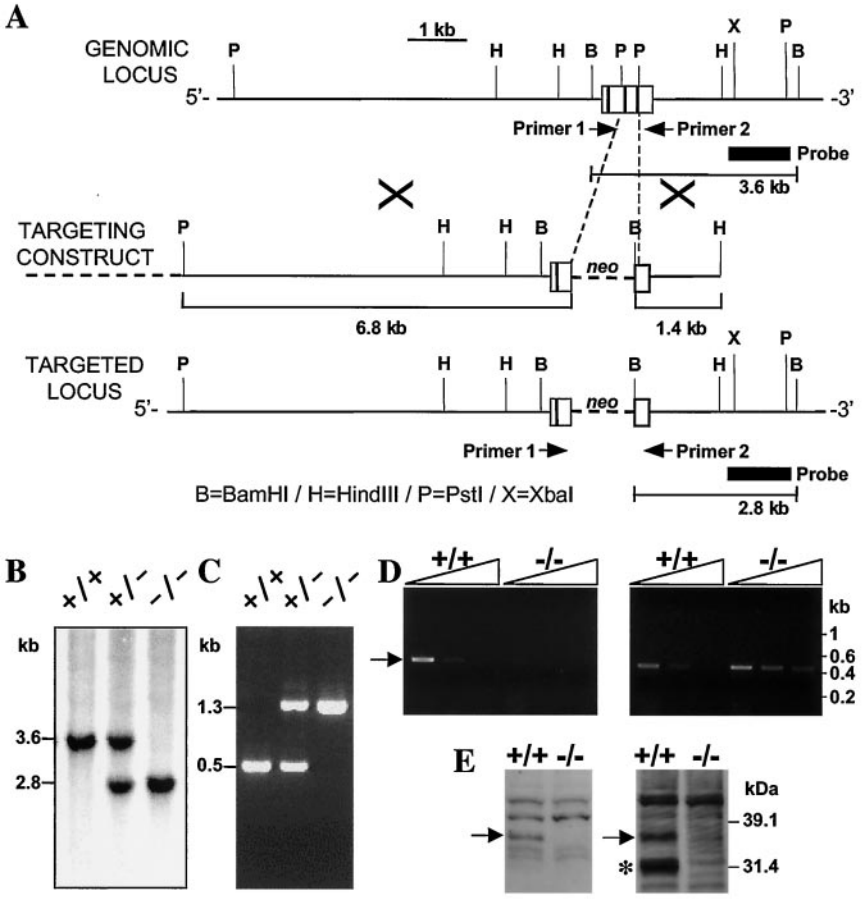

FIG. 1. Targeted disruption of murine *Trex1* locus. (A) Physical map of genomic DNA containing the *Trex1* gene. Genomic sequences are shown as a solid line, with the single *Trex1* coding exon depicted as an open box and the three conserved exonuclease motifs indicated by vertical black bars within it; vector sequences are shown with dashed lines. Genomic DNA fragments were subcloned on either side of a *neo* cassette to generate a construct that deleted sequences encoding amino acids 103 to 207 of the 304-amino-acid *Trex1* ORF product (including motifs II and III) at the targeted locus. Restriction digestion with BamHI gave rise to a 3.6-kb fragment at the wild-type locus and a 2.8-kb fragment at the targeted locus that were detected by hybridization with a 3′ flanking probe (filled box). The positions of sense and antisense PCR primers 1 and 2, which amplify a 0.5-kb wild-type product and a 1.3-kb product from the targeted locus, are indicated. Genotyping of representative wild-type (+/+), heterozygous (+/−), and *Trex1* null (−/−) live-born F2 progeny from tail-snip biopsy samples by Southern hybridization analysis with the 3′ probe (B) or by PCRs with primers 1 and 2 (C) is shown. (D) RT-PCR analysis of increasing amounts of total RNA (5, 50, and 500 ng) from spleens of wild-type (+/+) and *Trex1* null (−/−) mice. A Trex1-specific signal (arrow; same primers as for panel A) was detected for the wild-type but not the *Trex1* null mice (left); a signal for the glyceraldehyde-3-phosphate dehydrogenase control (see Materials and Methods) was readily detected in both wild-type and null samples (right). The migration of DNA markers (in kilobases) is shown. (E) Immunoblot analysis of MEF (left) and liver (right) nuclear protein extracts from wild-type (+/+) and *Trex1* null (−/−) mice with a murine Trex1-specific antipeptide antiserum. The migration of full-length Trex1 is indicated in each case (arrows); a Trex1 fragment for the wild-type liver is marked by an asterisk. The migration of molecular mass markers (in kilodaltons) is indicated.

for catalysis (14, 29). There are no introns within the ORF of the murine *Trex1* gene, as was also reported for the human and bovine genes (31). An analysis of the *Trex1* gene structure identified alternative transcripts that are generated through splicing of the 5′ flanking region and the use of different splice acceptor sites. A conserved methionine initiates a 314-amino-acid isoform in mice and humans. The 304-amino-acid product lacks the 10 N-terminal residues of the 314-amino-acid product and initiates at methionine 11, which is conserved in humans and mice. There was no difference in the enzymatic properties of the 304- versus 314-amino-acid recombinant human proteins, and both were poorly expressed from various plasmid constructs and largely insoluble in *E. coli* (30; also data not shown). An upstream ORF encoding the ATR-interacting protein ATRIP (8), apparently encoded by partially overlapping spliced mRNA transcripts from the same gene locus (http://www.ncbi.nih.gov/LocusLink/LocRpt.cgi?l=11277), would not be affected by homologous integration of the targeting construct here.

Two independent ES clones, in which one allele of the *Trex1* gene had been correctly targeted, were injected into host blastocysts to generate germ line chimeras and heterozygous *Trex1*$^{-/-}$ mice, and they gave identical results in all subsequent experiments. Genotyping of live-born mice from intermatings of F_1 heterozygotes by Southern hybridization or PCR analysis (Fig. 1B and C) showed that *Trex1*$^{-/-}$ homozygous null mice were viable and were recovered in F_2 litters according to Mendelian segregation. PCR amplification of reverse-transcribed total RNAs from wild-type and null spleens confirmed that the *Trex1* transcript was not produced in homozygous gene-tar-

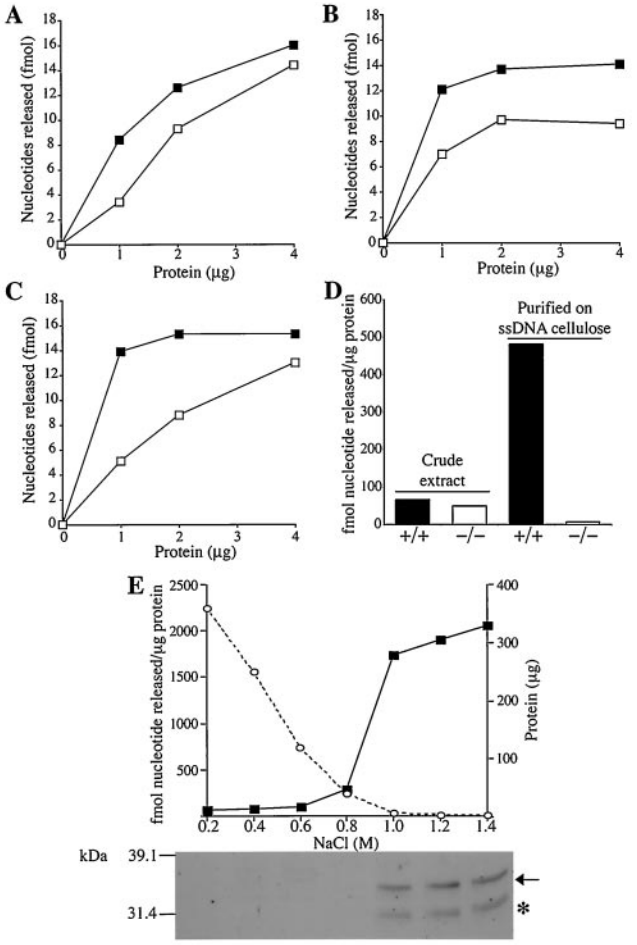

FIG. 2. DNA 3′ exonuclease activity in nuclear extracts of *Trex1*$^{-/-}$ and *Trex1*$^{+/+}$ cells and tissues. *Trex1*$^{-/-}$ (open boxes) and *Trex1*$^{+/+}$ (filled boxes) crude nuclear protein extracts from livers (A), testes (B), and thymus glands (C) were assayed for 3′ exonuclease activity with a 3′-end-labeled poly(dA) substrate. (D) Extracts from *Trex1*$^{-/-}$ (−/−) and *Trex1*$^{+/+}$ (+/+) MEF cell lines were assayed before and after partial purification by column chromatography on single-stranded DNA (ssDNA)–cellulose, as indicated. (E) An extract of *Trex1*$^{+/+}$ mouse liver was loaded onto a single-stranded DNA–cellulose column and eluted with increasing salt concentrations (as indicated). The protein fractions were quantified (open circles) and assayed as described above for 3′ exonuclease activity (filled boxes) and by immunoblotting with a specific antiserum which detects full-length Trex1 (arrow) and a proteolytic fragment (asterisk) (as in Fig. 1E).

geted mice (Fig. 1D). The PCR primers used were located within the ORF, spanning exonuclease motifs II and III (Fig. 1A). Thus, 5′ alternatively spliced forms were not differentiated and only a single product was seen for the wild type, while a transcript terminating at the polyadenylation signal of the *neo* cassette and lacking the second and third catalytic motifs could not be detected. Similarly, immunoblotting of protein extracts from *Trex1*$^{-/-}$ versus *Trex*$^{+/+}$ MEF cell lines and livers confirmed that the Trex1 gene product was not expressed in *Trex1* null mice (Fig. 1E). The antiserum was raised against a C-terminal peptide from the murine Trex1 protein and could not detect a hypothetical truncated inactive N-terminal product of the targeted gene. The 314-amino-acid murine Trex1 protein has a predicted molecular mass of 33,675 Da, migrates as an ~33-kDa polypeptide by sodium dodecyl sulfate-polyacrylamide gel electrophoresis, and gives rise to an active fragment with an apparent molecular mass of 30 kDa (30). In this study, the full-length protein was detected in wild-type MEFs and livers, while an ~31-kDa form was also seen in an extract of wild-type livers but not in the MEF cell line (Fig. 1E, right panel).

Reduced 3′ exonuclease activity in cell-free tissue extracts from *Trex1* null mice. TREX1 degrades single-stranded DNA in a nonprocessive manner from a 3′ terminus and was purified as the major 3′ exonuclease activity in a mammalian nuclear extract by a direct biochemical approach, as assayed with a 3′-end-labeled poly(dA) substrate (14). However, there are several 3′→5′ DNA exonucleases in mammalian cells that can act on this substrate (42). In a comparison of crude nuclear extracts of various tissues from *Trex1*$^{-/-}$ and *Trex*$^{+/+}$ mice under nonsaturating assay conditions, Trex1 appeared to account for 35 to 60% of the total 3′ exonuclease activity in a variety of tissues (Fig. 2A to C) and only ~25% of the activity in a rapidly dividing *Trex1*$^{+/+}$ MEF cell line (Fig. 2D, crude extract). However, after a partial purification of DNA-binding proteins from crude nuclear extracts by single-stranded DNA–cellulose chromatography, the 3′ exonuclease activity was greatly increased in a wild-type but not a Trex1-deficient MEF extract. Thus, the Trex1 enzyme accounted for ~99% of the total nuclear 3′ DNA exonuclease binding to single-stranded DNA–cellulose (Fig. 2D). Furthermore, the 3′ DNA exonuclease activity in fractions eluted with increasing salt concentrations from single-stranded DNA–cellulose was coincident with the presence of the Trex1 protein, as detected by immunoblotting (Fig. 2E).

Spontaneous mutation frequency is not increased in *Trex1* null mice. *Trex1*$^{-/-}$ null and *Trex1*$^{+/+}$ wild-type mice were established in a homozygous *Big Blue* background, such that spontaneous mutation frequencies could be determined for the *cII* transgene recovered from the livers of 5-week-old animals and packaged into viable bacteriophages. The numbers of *cII*$^{-}$ mutant plaques, the total numbers of PFU plated, and the calculated mutation frequencies are presented in Table 1. There was no significant difference in spontaneous mutation frequency observed in the livers of *Trex1*$^{-/-}$ and wild-type animals. The observed mutation frequency of the *cII* transgene in wild-type livers was approximately three times that observed for the *lacI* marker in the same strain background (19), with both values being in good agreement with those in previous studies (55). These data do not support a role for Trex1 in editing mismatched 3′ termini generated during DNA repair or DNA replication.

Reduced survival of Trex1-deficient mice. At weaning (~4 weeks), *Trex1*$^{-/-}$ mice were indistinguishable from their het-

TABLE 1. Spontaneous mutation frequencies in livers from *Big Blue*/*TREX*$^{+/+}$ and *Big Blue*/*Trex1*$^{-/-}$ mice

Genotype	No. of PFU plated	No. of *cII*$^{-}$ mutants	Frequency (10^{-5})	Mean (10^{-5})
+/+	461,000	50	10.85	9.78
	598,000	52	8.70	
−/−	498,000	52	10.44	9.98
	524,000	53	10.12	
	547,000	51	9.37	

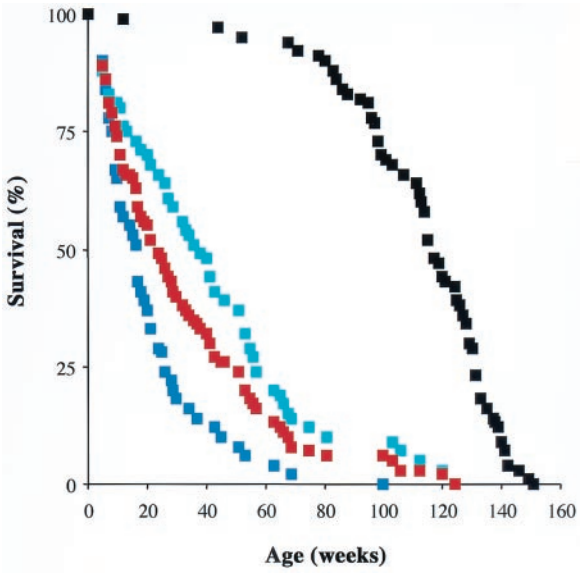

FIG. 3. Reduced survival of *Trex1* null mice. Survival curves are shown for all *Trex1*$^{-/-}$ mice in this study (n = 110; red curve) and for the wild-type *Trex1*$^{+/+}$ controls (n = 77; black curve). For those *Trex1*$^{-/-}$ mice that were born to heterozygous (n = 51; dark blue curve) or homozygous null (n = 59; light blue curve) mothers, the difference in median survival of 21 weeks was significant (log rank test with 95% confidence interval; $P < 0.0001$).

erozygous and wild-type littermates. However, there was a dramatically increased morbidity of *Trex1* null mice postweaning. Figure 3 shows survival data for a total of 110 *Trex1*$^{-/-}$ mice that were monitored until death in this study; data for *Trex1*$^{+/+}$ control mice, kept under identical conditions and over the same time period, are shown for comparison and have been published previously (34). The median time of survival was reduced from >2 years (116 weeks), as is normally seen for this wild-type strain background, to ~6 months. Interestingly, there was a significant difference in the survival of *Trex1*$^{-/-}$ progeny from heterozygous versus homozygous null matings, with an increased morbidity for *Trex1* null mice born to heterozygous mothers (50% survival at 17 weeks) compared to that for mice born to homozygous null mothers (50% survival at 38 weeks). There was no significant difference in the ratios of female to male mice for the two groups (~0.58 for both groups) or in the cumulative numbers of deaths for female versus male mice. Only ~5% of all *Trex1*$^{-/-}$ mice in this study survived beyond 2 years, with the oldest surviving to 124 weeks; these were all born to homozygous null mothers. All control mice were the progeny of F_2 heterozygotes from 129Sv-C57BL/6J chimera × C57BL/6J matings. Because of the dramatically reduced survival of *Trex1*$^{-/-}$ mice, it was not possible to breed a large number from the same generation; the mice used in this study were from generations F_2 to F_4 (heterozygous matings) or F_3 to F_5 (homozygous matings).

Cardiomyopathy and circulatory failure in Trex1-deficient mice. Mice were examined macroscopically postmortem, and 61% of deaths in *Trex*$^{-/-}$ mice were found to be due to circulatory failure. Typically, there was a thrombus formation in one or both auricles, with fluid in the thorax and congestion of the lungs. The affected auricle(s) was often enlarged, and in some instances cardiomyopathy was indicated by diffuse areas of a grayish discoloration in the cardiac muscle; necrotic areas on the liver or kidneys were occasionally noted. Strikingly, in about one-third of the deaths due to circulatory failure, there was also a massive distension of the whole heart to two to three times the normal size (Fig. 4A). Cardiomyopathy and circulatory failure were reported more frequently in postmortem reports for *Trex1*$^{-/-}$ mice born to heterozygous mothers than for those born to homozygous null mothers (73% versus 51%), and this was consistent with the observed difference in survival (Fig. 3). The increased morbidity of *Trex1*$^{-/-}$ mice was most marked from weaning until 20 weeks of age (Fig. 3) and either was due to circulatory failure or had no identifiable pathology but occurred soon after weaning. For a substantial proportion of all *Trex1* null deaths (~20%), a clear cause was not discernible macroscopically; half of these animals were <3 months old. Although it was not the only cause of death in older null mice, circulatory failure remained a major factor and was seen in animals as old as 2 years. In older mice, the only other recurrent pathology was an enlargement of the spleen and/or lymph nodes in <10% of the mice, predominantly in those older than 1 year, with lymphoma observed in <1% of the mice; this was also seen in control mice and is within normal limits for this strain background (34). There was no detectable increase in the frequency of solid tumors in *Trex1*$^{-/-}$ mice.

Histopathology of inflammatory myocarditis and progressive dilated cardiomyopathy in Trex1-deficient mice. Systematic histopathological analyses were carried out with *Trex1*$^{-/-}$ mice that had shown the typical null phenotype of auricular thrombus, cardiomyopathy, and circulatory failure upon macroscopic inspection. Initially, two female mice who had died at 10 to 12 weeks of age, one with an enlarged heart and greatly distended auricles, were examined; a wild-type female littermate of one of the affected mice from a heterozygous cross was sacrificed for comparison. Another *Trex1* null mouse, for which a macroscopic examination had indicated a more extreme pathology, with a mottled white appearance to the ventricles (observed to a lesser degree in other cases) and a rupture of the heart muscle, was also examined. For the *Trex1* null mice, histological examination confirmed an organizing thrombus within the atrium, with inflammation of the endothelium extending into the muscle wall, active myocarditis that was maximal within the endothelial-subendocardial zones, and myocyte degeneration with edema between muscle fibers (Fig. 4B and C). A normal heart is shown in the figure for comparison (Fig. 4D). The inflammatory infiltrate in the heart consisted of a mixed population of lymphoid cells, including neutrophils and mononucleocytes. Immunostaining identified predominantly CD3-positive T cells, although some B cells expressing CD45R were also present (Fig. 4E and F).

The observed inflammatory myocarditis was not due to an increased susceptibility to cardiotoxic viruses, such as murine cytomegalovirus or minute virus of mice; progeny born to *Trex1* null mice with a verified health status after rederivation (by sterile embryo transfer into clean foster mothers) continued to die prematurely of heart failure. Four such mice (two males and two females) that died at 6 to 8 weeks were examined and showed the same histopathology as that described above. In addition to the inflammatory myocarditis, there was a secondary vascular congestion of the lungs and liver. Furthermore, in

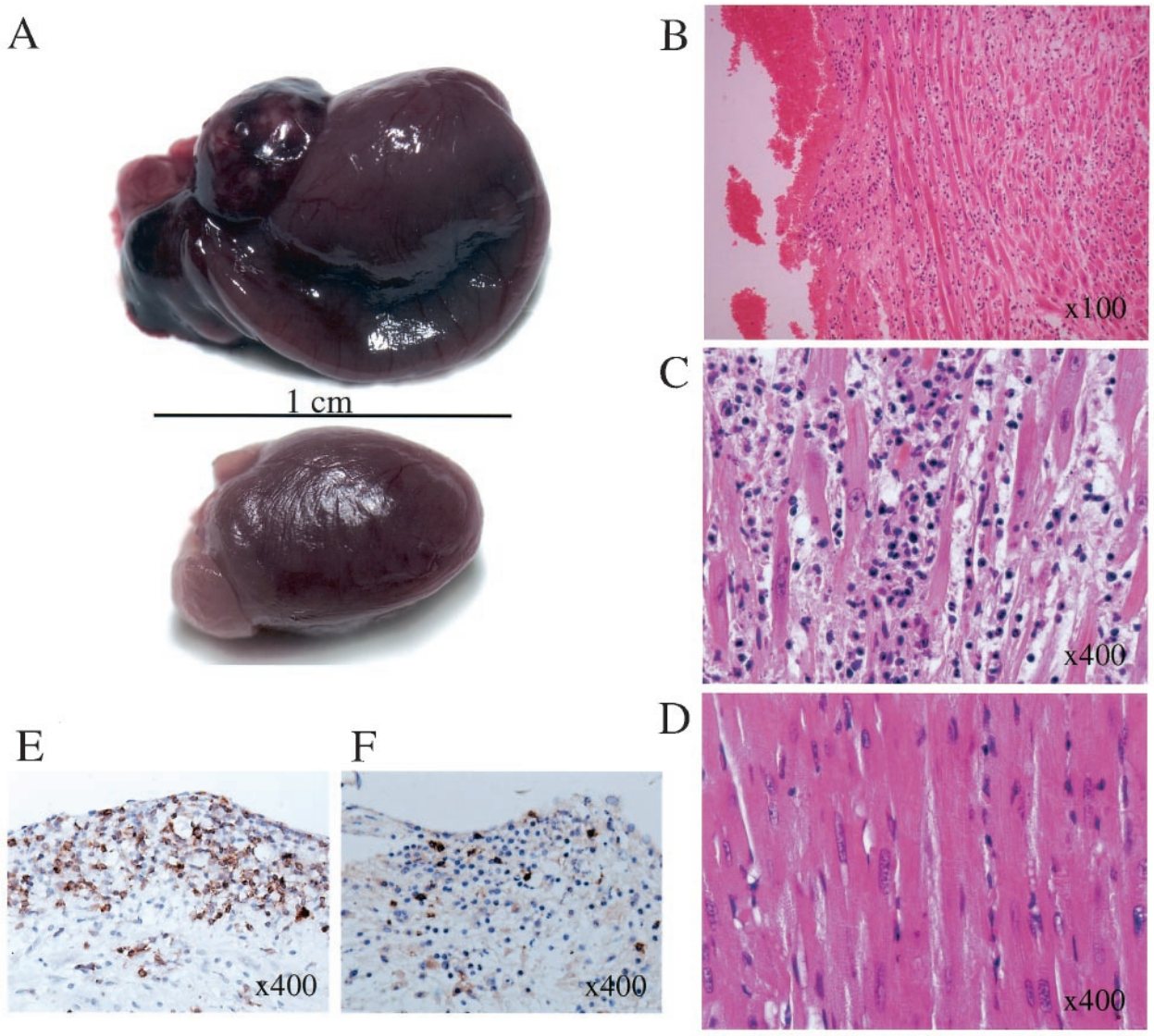

FIG. 4. Heart pathology in *Trex1* null mice. (A) Auricular thrombus and distended heart in a *Trex1*$^{-/-}$ female mouse that died of circulatory failure at 40 weeks; the heart from a female control sacrificed at the same age is shown for comparison below. (B and C) Section through left auricle of affected 10-week-old animal (hematoxylin-eosin staining). (B) The normal myocardial muscle pattern is disrupted, with the red fibers being separated by a cellular inflammatory infiltrate with edema. The endocardial surface has a layer of adherent thrombus (left side of field). (C) At a higher magnification, the cardiac fibers appear to be degenerate, with a mixed infiltrate of dark lymphoid cells and polymorphs; (D) a normal control is shown for comparison. (E and F) Immunostaining of infiltrating lymphoid cells in a *Trex1*$^{-/-}$ heart shows predominantly CD3-positive T cells in the myocardium and the subendocardial region (E), with some CD45R-expressing B cells present as mainly perivascular aggregates in the subendocardial region (F); relatively few morphologically identifiable plasma cells were present. A scale bar and original magnifications are shown.

the majority of cases the spleen showed enlarged B-cell follicles and indistinct marginal zones. There were also focal lymphoid aggregates seen in the liver, lungs, and other tissues. Notably, in two of three *Trex1* null mice in which it was examined, the thymus showed cortical atrophy (Fig. 5). Four further control *Trex1*$^{+/+}$ animals, in which there had been minor cardiac abnormalities, including a possible slight enlargement, a small thrombus, and pericardial bleeding, upon macroscopic postmortem inspection, were examined. For none of these cases was there any indication of myocarditis, structural abnormality, or active inflammation (except in one case for which epicardial inflammation could be attributed to chronic renal failure).

DISCUSSION

We generated homozygous null mice that were deficient in the 3′→5′ DNA exonuclease Trex1. An analysis of the exonuclease activities in nuclear extracts of various organs and MEFs from null mice confirmed that Trex1 is the major 3′→5′ DNA exonuclease in nonproliferating, as well as proliferating, mammalian cells. *Trex1*$^{-/-}$ mice were viable and showed no increase in spontaneous mutation frequency. A DNA-editing role for TREX1 had been proposed, particularly in regard to base excision repair (14, 30). However, the present data demonstrate that Trex1 does not act in base excision repair or else is redundant with other 3′ exonuclease activities which may

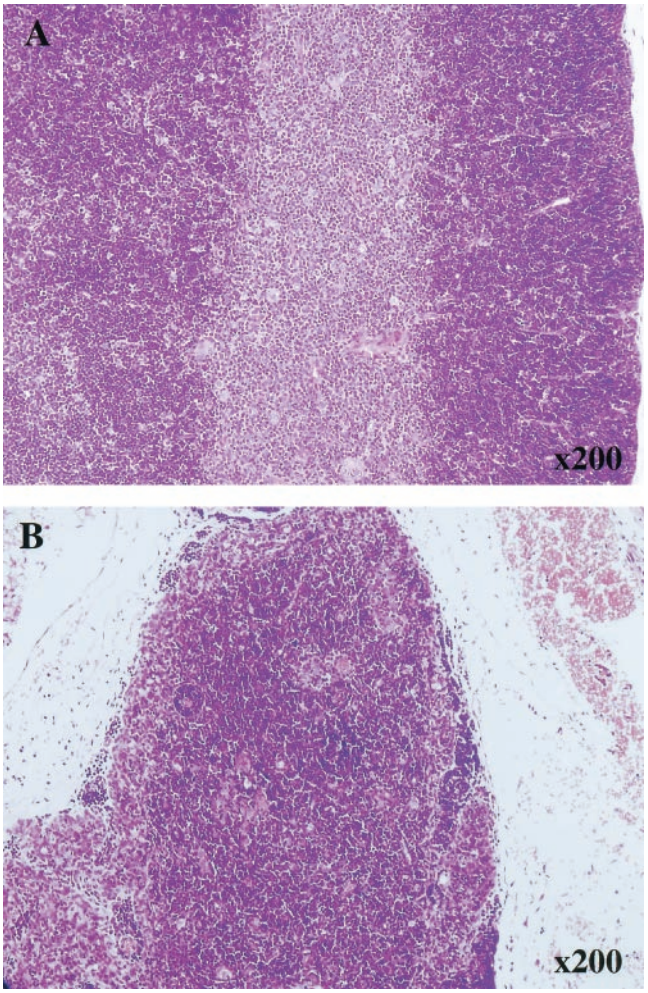

FIG. 5. Thymus pathology in *Trex1* null mice. (A) Normal thymus from a $Trex1^{+/+}$ control shows clear distinction between the darker lymphocyte-rich cortex and the paler medulla. (B) Atrophic thymus from a representative $Trex1^{-/-}$ mouse has indistinct corticomedullary junction and is smaller overall. The mice were females 10 to 12 weeks old. Original magnifications are indicated.

fulfill this editing role, such as that associated with the mammalian AP endonuclease (5, 51). In an unexpected result, *Trex1* null mice showed a dramatically reduced survival that was associated with the development of inflammatory myocarditis, progressive cardiomyopathy, and circulatory failure.

Cardiomyopathies are usually associated with defects in structural components or calcium ion regulation in the heart and are the most common cause of heart failure (for a recent commentary, see reference 28). In *Trex1* null mice, cardiomyopathy and heart failure occured secondarily to an inflammatory myocarditis. In humans, myocarditis is most commonly caused by viral infections (12, 26), but it can also be linked to bacterial infections through antigenic mimicry (1) and is modulated by proinflammatory cytokines (11). Experimental mouse models have similarly relied on coxsackievirus infections, immunization with cardiac myosin, or transgene-mediated cytokine overexpression. Here we have shown that a deficiency in the ubiquitous nuclear 3′→5′ DNA exonuclease Trex1 unexpectedly leads to the spontaneous development of inflammatory myocarditis in pathogen-free mice. The *Trex1* null phenotype is strikingly similar to that of murine models of organ-specific autoimmune myocarditis and dilated cardiomyopathy generated by the genetic manipulation of cell surface molecules known to act in the immune system (9, 35). Thus, in specific genetic backgrounds, transgenic expression of the human diabetes-associated histocompatibility antigen HLA-DQ8 (9) or deletion of the PD-1 immunoreceptor involved in peripheral tolerance (35) caused autoimmune cardiomyopathy. In the former instance, there was an infiltration of mononuclear cells in the myocardium and a postinflammatory dilated cardiomyopathy, which are typical of the human idiopathic disease, leading to heart failure from 20 weeks of age (9). A similar histopathological picture was seen for *Trex1* null mice (Fig. 4), although, like the *PD-1* knockout (35), $Trex1^{-/-}$ mice died as early as 5 weeks, with about two-thirds of them being dead by 30 weeks (Fig. 3).

The inflammatory myocarditis observed in Trex1-deficient mice could be consistent with an autoimmune disease. Autoimmune cardiomyopathy has been correlated with a loss of peripheral tolerance to autoreactive T cells in PD-1 receptor-deficient mice. However, depending on the strain background, the immune defect can be manifested as a lupus-like disease in $PD\text{-}1^{-/-}$ mice (35), and systemic lupus erythematosus (SLE) is associated with a polymorphism in the human *PD1* gene (39). Autoantibodies to various nuclear constituents are often produced in autoimmune diseases and are the hallmark of SLE, although this is a highly complex and multifactorial disorder (for a recent commentary, see reference 27). DNA itself is a poor antigen, but anti-Ig autoantibodies are produced in response to IgG bound to chromatin (21) or DNA-containing hypomethylated CpG motifs (46). Interestingly, the pancreatic lysosomal endonuclease DNase I is apparently responsible for the clearance of DNA from nuclear antigens released by cell turnover; the *DNase I* gene is mutated in some SLE patients (52) and features of SLE are recapitulated in DNase I-deficient mice (32). Similarly, the inability of mice deficient in macrophage lysosomal DNase enzymes to clear DNA from apoptotic cells can activate innate immunity, leading to defects in thymic development (18) or an increased susceptibility to SLE (49). However, the nuclear localization and absence of endonuclease activity of the TREX1 3′→5′ exonuclease are not consistent with such a role. Furthermore, the murine *Trex1* gene does not appear to correspond to known loci that predispose lupus-prone mice to autoimmunity (45, 49). Intriguingly, the 3′ exonuclease activity of the mammalian AP endonuclease is enhanced in a truncated form that is associated with chromatin fragmentation during apoptosis (53), and the APE1 protein is a target of the cytotoxic T-lymphocyte granzyme A-mediated cell death pathway (10).

Cardiomyopathy can also accompany increases in mitochondrial DNA mutations, as seen in transgenic mice with cardiac-specific expression of a proofreading-deficient mitochondrial DNA Polγ (54). However, TREX1 is a nuclear protein (14) and might not be expected to contribute to the integrity of the mitochondrial genome. There is no increase in spontaneous mutagenesis in *Trex1* null mice and no cytogenetic evidence for increased instability of the nuclear genome, as levels of sister chromatid exchanges were within the normal range in $Trex1^{-/-}$

MEFs (data not shown). Consistent with the resistance of free radical-generated 3′ phosphoglycolate DNA ends to digestion by TREX1 (16), *Trex1*$^{-/-}$ MEFs did not show an increased sensitivity to hydrogen peroxide or γ-irradiation (data not shown). Similarly, the TREX1 excision activity is blocked by bulky lesions in the DNA (24). The phosphorylation of p53 after UV radiation (17) was seen in both *Trex1*$^{-/-}$ and *Trex1*$^{+/+}$ MEFs, indicating that the ATR-mediated DNA damage checkpoint is intact and that the function of the upstream ATRIP gene is unaffected in *Trex1* null mice (data not shown). Thus, although the expression of TREX1 is consistent with a DNA repair- rather than DNA replication-associated enzyme (14, 31), there is currently no direct evidence for a role of TREX1 in DNA repair. However, TREX1 may have a role in DNA recombination. For example, the 3′→5′ exonuclease activity associated with terminal deoxynucleotidyltransferase has been shown to catalyze the deletion of nucleotides at coding joints during V(D)J recombination of Ig and T-cell receptor genes during diversification of the immune system (44).

In addition to developing inflammatory myocarditis and dilated cardiomyopathy, *Trex1* null mice also showed pathological changes in the lymphoid organs, in both the spleen and the thymus. Moreover, there was a significantly increased morbidity for Trex1-deficient mice born to heterozygous mothers than for those born to homozygous null mothers. This could indicate a transfer of autoantibodies in the milk (9) from *Trex1*$^{-/-}$ mothers that exacerbates the null phenotype in *Trex1*$^{-/-}$ progeny. We cannot formally rule out that a stable truncated N-terminal fragment of the Trex1 protein may be produced in the *Trex1*$^{-/-}$ null mice and could act as an autoantigen. However, Trex1 is uniformly expressed in all tissues, not just the heart (31), and at a low level (14, 29), so we consider this an unlikely possibility. Our data indicate that Trex1 might have a previously unrecognized function either in or affecting the immune system and cannot be replaced in this capacity by another mammalian 3′→5′ DNA exonuclease. Although the mechanistic basis has yet to be elucidated, a role for the 3→5 exonuclease activity of TREX1 could be envisioned in the processing of DNA termini during a subset of V(D)J recombination events, receptor editing, or class-switch recombination. Analyses of Ig junction sequences in *Trex1*$^{-/-}$ mice and of the null phenotype in a genetic background in which V(D)J recombination (4) or isotype switching (40) is inhibited will be the first steps in indicating whether and where Trex1 acts in the normal functioning of the immune system. Interestingly, it has been determined that 55 to 75% of antibodies emerging in the bone marrow are self reactive, and the primary cause of autoantibody formation is random nucleotide addition and deletion during diversification of Ig heavy chains (47). Receptor editing allows B cells to alter their receptor specificities upon encountering antigens, apparently by the processing of DNA ends during continued RAG-mediated V(D)J recombination, to increase their repertoire but also as a means of maintaining tolerance (33, 41).

TREX1 is expressed in all mammalian tissues examined (14, 29, 31), but its ubiquitous role in the cell nucleus remains unclear. TREX1 is a small polypeptide with a catalytic domain encompassing three conserved exonuclease motifs, but it has a unique extended C terminus that has no homology to other 3′ exonucleases. An orthologue of the TREX1/2 exonuclease domain has been identified in *Drosophila* (31) and from expressed sequence tag databases in *Ciona* and *Xenopus* (data not shown), but the TREX1/2 gene duplication and the extended TREX1 C-terminal region are documented only for mammals. Deletion of the *Trex1* gene from mice unexpectedly resulted in the development of inflammatory myocarditis. Future work will seek to identify putative protein partners that might interact with the unique C-terminal region of TREX1 and target the protein to a previously unrecognized role revealed by the murine *Trex1* null phenotype. It might also be pertinent now to search for inherited *TREX1* mutations in myocarditis patients with a family history of the disease.

ACKNOWLEDGMENTS

We thank Ashfaq Gilkar and Mahrokh Nohadani for histopathology, Christine Saunders and Russell Sanderson for work with MEF cell lines, Tania Jones for sister chromatid exchange analyses, Michael Bradburn for assistance with statistical analysis, Michael Mitchell for database searches, and Mary Ann Haskings, Anthony Iglesias, Barbara Rudling, Del Watling, Stephen Wilson, and Cheryl Young for technical assistance. We thank Susumu Nishimura for facilitating a long-term visit of M.M. to the Clare Hall laboratories.

This work was supported by Cancer Research UK.

REFERENCES

1. **Bachmaier, K., J. Le, and J. M. Penninger.** 2000. "Catching heart disease": antigenic mimicry and bacterial infections. Nat. Med. **6:**841–842.
2. **Bennett, R. A., D. M. Wilson, D. Wong, and B. Demple.** 1997. Interaction of apurinic endonuclease and DNA polymerase β in the base excision repair pathway. Proc. Natl. Acad. Sci. USA **94:**7166–7169.
3. **Brown, K. R., K. L. Weatherdon, C. L. Galligan, and V. Skalski.** 2002. A nuclear 3′-5′ exonuclease proofreads for the exonuclease-deficient DNA polymerase α. DNA Repair **1:**795–810.
4. **Chen, J., R. Lansford, V. Stewart, F. Young, and F. W. Alt.** 1993. RAG-2-deficient blastocyst complementation: an assay of gene function in lymphocyte development. Proc. Natl. Acad. Sci. USA **90:**4528–4532.
5. **Chou, K.-M., and Y.-C. Cheng.** 2002. An exonucleolytic activity of human apurinic/apyrimidinic endonuclease on 3′ mispaired DNA. Nature **415:**655–659.
6. **Chou, K.-M., and Y.-C. Cheng.** 2003. The exonuclease activity of human apurinic/apyrimidinic endonuclease (APE1). J. Biol. Chem. **278:**18289–18296.
7. **Chou, K.-M., M. Kukhanova, and Y.-C. Cheng.** 2000. A novel action of human apurinic/apyrimidinic endonuclease. J. Biol Chem. **275:**31009–31015.
8. **Cortez, D., S. Guntuku, J. Qin, and S. J. Elledge.** 2001. ATR and ATRIP: partners in checkpoint signaling. Science **294:**1713–1716.
9. **Elliott, J. F., J. Liu, Z.-N. Yuan, N. Bautista-Lopez, S. L. Wallbank, K. Suzuki, D. Rayner, P. Nation, M. A. Robertson, G. Liu, and K. M. Kavanagh.** 2003. Autoimmune cardiomyopathy and heart block develop spontaneously in HLA-DQ8 transgenic IAβ knockout NOD mice. Proc. Natl. Acad. Sci. USA **100:**13447–13452.
10. **Fan, Z., P. J. Beresford, D. Zhang, Z. Xu, C. D. Novina, A. Yoshida, Y. Pommier, and J. Lieberman.** 2003. Cleaving the oxidative repair protein Ape1 enhances the cell death mediated by granzyme A. Nat. Immunol. **4:**145–153.
11. **Feldman, A. M., A. Combes, D. Wagner, T. Kadakomi, T. Kubota, Y. Y. Li, and C. McTiernan.** 2000. The role of tumor necrosis factor in the pathophysiology of heart failure. J. Am. Coll. Cardiol. **35:**537–544.
12. **Gauntt, C., and S. Huber.** 2003. Coxsackievirus experimental heart diseases. Front. Biosci. **8:**E23–E35.
13. **Goldsby, R. E., N. A. Lawrence, L. E. Hays, E. A. Olmsted, X. Chen, M. Singh, and B. D. Preston.** 2001. Defective DNA polymerase-δ proofreading causes cancer susceptibility in mice. Nat. Med. **7:**638–639.
14. **Höss, M., P. Robins, T. J. P. Naven, D. J. C. Pappin, J. Sgouros, and T. Lindahl.** 1999. A human DNA editing enzyme homologous to the *Escherichia coli* DnaQ/MutD protein. EMBO J. **18:**3868–3875.
15. **Huang, S., L. Baomin, M. D. Gray, J. Oshima, S. Mian, and J. Campisi.** 1998. The premature aging syndrome protein, WRN, is a 3′→5′ exonuclease. Nat. Genet. **20:**114–116.
16. **Inamdar, K. V., Y. Yu, and L. F. Povirk.** 2002. Resistance of 3′-phosphoglycolate DNA ends to digestion by mammalian DNase III. Radiat. Res. **157:**306–311.
17. **Kapoor, M., and G. Lozano.** 1998. Functional activation of p53 via phosphorylation following DNA damage by UV but not γ radiation. Proc. Natl. Acad. Sci. USA **95:**2834–2837.

18. **Kawane, K., H. Fukuyama, H. Yoshida, H. Nagase, Y. Ohsawa, Y. Uchiyama, K. Okada, T. Iida, and S. Nagata.** 2003. Impaired thymic development in mouse embryos deficient in apoptotic DNA degradation. Nat. Immunol. **4:**138–144.
19. **Klungland, A., I. Rosewell, S. Hollenbach, E. Larsen, G. Daly, B. Epe, E. Seeberg, T. Lindahl, and D. E. Barnes.** 1999. Accumulation of premutagenic DNA lesions in mice defective in removal of oxidative base damage. Proc. Natl. Acad. Sci. USA **96:**13300–13305.
20. **Larsen, E., C. Gran, B. E. Saether, E. Seeberg, and A. Klungland.** 2003. Proliferation failure and gamma radiation sensitivity of Fen1 null mutant mice at the blastocyst stage. Mol. Cell. Biol. **23:**5346–5353.
21. **Leadbetter, E. A., I. R. Rifkin, A. M. Hohlbaum, B. C. Beaudette, M. J. Shlomchik, and A. Marshak-Rothstein.** 2002. Chromatin-IgG complexes activate B cells by dual engagement of IgM and Toll-like receptors. Nature **416:**603–607.
22. **Lebedeva, N. A., S. N. Khodyreva, A. Favre, and O. I. Lavrik.** 2003. AP endonuclease 1 has no biologically significant 3′→5′ exonuclease activity. Biochem. Biophys. Res. Commun. **300:**182–187.
23. **Lieber, M. R.** 1997. The FEN-1 family of structure-specific nucleases in eukaryotic DNA replication, recombination and repair. Bioessays **19:**233–240.
24. **Lindahl, T.** 1971. Excision of pyrimidine dimers from ultraviolet-irradiated DNA by exonucleases from mammalian cells. Eur. J. Biochem. **18:**407–414.
25. **Lindahl, T., J. A. Gally, and G. M. Edelman.** 1969. Properties of deoxyribonuclease III from mammalian tissues. J. Biol. Chem. **244:**5014–5019.
26. **Maisch, B., A. D. Ristic, I. Portig, and S. Pankuweit.** 2003. Human viral cardiomyopathy. Front. Biosci. **8:**S39–S67.
27. **Marshall, E.** 2002. Lupus: mysterious disease holds its secrets tight. Science **296:**689–691.
28. **Marx, J.** 2003. How to subdue a swelling heart. Science **300:**1492–1496.
29. **Mazur, D. J., and F. W. Perrino.** 1999. Identification and expression of the TREX1 and TREX2 cDNA sequences encoding mammalian 3′→5′ exonucleases. J. Biol. Chem. **274:**19655–19660.
30. **Mazur, D. J., and F. W. Perrino.** 2001. Excision of 3′ termini by the Trex1 and TREX2 3′→5′ exonucleases. J. Biol. Chem. **276:**17022–17029.
31. **Mazur, D. J., and F. W. Perrino.** 2001. Structure and expression of the TREX1 and TREX2 3′→5′ exonuclease genes. J. Biol. Chem. **276:**14718–14727.
32. **Napirei, N., H. Karsunky, B. Zevnik, H. Stephan, H. G. Mannherz, and T. Möröy.** 2000. Features of systemic lupus erythematosus in Dnase1-deficient mice. Nat. Genet. **25:**177–181.
33. **Nemazee, D., and M. Weigert.** 2000. Revising B cell receptors. J. Exp. Med. **191:**1813–1817.
34. **Nilsen, H., G. Stamp, S. Andersen, G. Hrivnak, H. E. Krokan, T. Lindahl, and D. E. Barnes.** 2003. Gene-targeted mice lacking the Ung uracil-DNA glycosylase develop B-cell lymphomas. Oncogene **22:**5381–5386.
35. **Nishimura, H., T. Okazaki, Y. Tanaka, K. Nakatani, M. Hara, A. Matsumori, S. Sasayama, A. Mizoguchi, H. Hiai, N. Minato, and T. Honjo.** 2001. Autoimmune dilated cardiomyopathy in PD-1 receptor-deficient mice. Science **291:**319–322.
36. **Perrino, F. W., and L. A. Loeb.** 1989. Proofreading by the ε subunit of Escherichia coli DNA polymerase III increases the fidelity of calf thymus DNA polymerase α. Proc. Natl. Acad. Sci. USA **86:**3085–3088.
37. **Perrino, F. W., D. J. Mazur, H. Ward, and S. Harvey.** 1999. Exonucleases and the incorporation of aranucleotides into DNA. Cell. Biochem. Biophys. **30:**331–352.
38. **Perrino, F. W., H. Miller, and K. A. Ealey.** 1994. Identification of a 3′→5′ exonuclease that removes cytosine arabinoside monophosphate from 3′ termini of DNA. J. Biol. Chem. **269:**16357–16363.
39. **Prokunina, L., C. Castillejo-López, F. Öberg, I. Gunnarsson, L. Berg, V. Magnusson, A. J. Brookes, D. Tentler, H. Kristjansdóttir, G. Gröndal, A. I. Bolstad, E. Svenungsson, I. Lundberg, G. Sturfelt, A. Jönssen, L. Truedsson, G. Lima, J. Alcocer-Varela, R. Jönssen, U. B. Gyllensten, J. B. Harley, D. Alarcón-Segovia, K. Steinsson, and M. E. Alarcón-Riquelme.** 2002. A regulatory polymorphism in *PDCD1* is associated with susceptibility to systemic lupus erythematosus in humans. Nat. Genet. **32:**666–669.
40. **Rada, C., G. T. Williams, H. Nilsen, D. E. Barnes, T. Lindahl, and M. S. Neuberger.** 2002. Immunoglobulin isotype switching is inhibited and somatic hypermutation perturbed in UNG-deficient mice. Curr. Biol. **12:**1748–1755.
41. **Radic, M. Z., and M. Zouali.** 1996. Receptor editing, immune diversification, and self-tolerance. Immunity **5:**505–511.
42. **Shevelev, I. V., and U. Hübscher.** 2002. The 3′-5′ exonucleases. Nat. Rev. Mol. Cell. Biol. **3:**364–375.
43. **Shevelev, I. V., N. V. Belyakova, T. P. Kravetskaya, and V. M. Krutyakov.** 2000. Autonomous 3′→5′ exonucleases can proofread for DNA polymerase β from rat liver. Mutat. Res. **459:**237–242.
44. **Thai, T.-H., M. M. Purugganan, D. B. Roth, and J. F. Kearney.** 2002. Distinct and opposite diversifying activities of terminal transferase splice variants. Nat. Immunol. **3:**457–462.
45. **Vidal, S., D. H. Kono, and A. N. Theofilopoulos.** 1998. Loci predisposing to autoimmunity in MRL-*FAS*^{lpr} and C57BL/6-*FAS*^{lpr} mice. J. Clin. Investig. **101:**696–702.
46. **Viglianti, G. A., C. M. Lau, T. M. Hanley, B. A. Miko, M. J. Schlomchik, and A. Marshak-Rothstein.** 2003. Activation of autoreactive B cells by CpG dsDNA. Immunity **19:**837–847.
47. **Wardemann, H., S. Yurasov, A. Schaefer, J. W. Young, E. Meffre, and M. C. Nussenweig.** 2003. Predominant autoantibody production by early human B cell precursors. Science **301:**1374–1377.
48. **Wei, K., A. B. Clark, E. Wong, M. F. Kane, D. J. Mazur, T. Parris, N. K. Kolas, R. Russell, H. Hou, B. Kneitz, G. Yang, T. A. Kunkel, R. D. Kolodner, P. E. Cohen, and W. Edelmann.** 2003. Inactivation of exonuclease 1 in mice results in DNA mismatch repair defects, increased cancer susceptibility, and male and female sterility. Genes Dev. **17:**603–614.
49. **Wilber, A., T. P. O'Connor, M. L. Lu, A. Karimi, and M. C. Schneider.** 2003. Dnase 1l3 deficiency in lupus-prone MRL and NZB/W F1 mice. Clin. Exp. Immunol. **134:**46–52.
50. **Wong, D., and B. Demple.** 2004. Modulation of the 5-deoxyribose-5-phosphate lyase and DNA synthesis activities of mammalian DNA polymerase β by AP endonuclease I. J. Biol. Chem. **279:**25268–25275.
51. **Wong, D., M. S. DeMott, and B. Demple.** 2003. Modulation of the 3′→5′-exonuclease activity of human apurinic endonuclease (Ape1) by its 5′ incised abasic DNA product. J. Biol. Chem. **278:**36242–36249.
52. **Yasutomo, K., T. Horiuchi, S. Kagami, H. Tsukamoto, C. Hashimura, M. Urushihara, and Y. Kuroda.** 2001. Mutations of *DNASE1* in people with systemic lupus erythematosus. Nat. Genet. **28:**313–314.
53. **Yoshida, A., Y. Urasaki, M. Waltham, A.-C. Bergman, P. Pourquier, D. G. Rothwell, M. Inuzuka, J. N. Weinstein, T. Ueda, E. Apella, I. D. Hickson, and Y. Pommier.** 2003. Human apurinic/apyrimidinic endonuclease (Ape1) and its N-terminal truncated form (AN34) are involved in DNA fragmentation during apoptosis. J. Biol. Chem. **278:**37768–37776.
54. **Zhang, D., J. L. Mott, S.-W. Chang, G. Denniger, Z. Feng, and H. P. Zassenhaus.** 2000. Construction of transgenic mice with tissue-specific acceleration of mitochondrial DNA mutagenesis. Genomics **69:**151–161.
55. **Zimmer, D. M., P. R. Harbach, W. B. Mattes, and C. S. Aaron.** 1999. Comparison of mutant frequencies at the transgenic lambda *LacI* and *cII*/*cI* loci in control and ENU-treated Big Blue mice. Environ. Mol. Mutagen. **33:**249–256.